Proceedings 10th NUMGE 2023
10th European Conference on Numerical Methods in Geotechnical Engineering
Zdravkovic L, Kontoe S, Taborda DMG, Tsiampousi A (eds)

https://doi.org/10.53243/NUMGE2023-354

Numerical modelling of tides in an embankment lifecycle analysis

B.W.L. Guo[1,2], L.T. Zdravkovic[2], A. Tsiampousi[2], C.J. Onof[2], D.M. Potts[2]

[1]*Geotechnical Consulting Group, London, UK*
[2]*Department of Civil and Environmental Engineering, Imperial College, London, UK*

ABSTRACT: With constant exposure to the natural environment, flood embankments tend to deteriorate over their design life. To predict the performance and deterioration rate of a flood embankment, a complete lifecycle analysis is necessary, usually performed with advanced finite element computations. Due to the complexities of the numerical model and the long timescale of decades involved in a lifecycle analysis, it is challenging to take into consideration the impact of the constant semidiurnal tidal changes on the embankment stability and serviceability. This paper first models the impact of semidiurnal tidal changes on a typical flood embankment in the Thames estuary using a fine time-scale of hourly incremental changes over the period of one month. Subsequently, a simplified tidal cycle over one month is developed, with the aim of replicating the overall impact of the semidiurnal tides over one month with larger increments of time, in order to optimise the computational effort.

Keywords: Embankments; Tides; Lifecycle Analysis; Finite Elements.

1 INTRODUCTION

The stability of a flood embankment is typically assessed against a range of still water levels, from extreme low waters to extreme high waters (BSI, 2016). The extreme levels are usually determined from a combination of phenomena that influence water levels, such as storm surges, tides, seiches, or freshwater flow.

While this steady state approach gives a good understanding of the performance of an embankment subjected to an extreme water level, it does not consider the reality of that embankment being subjected to constant hydraulic changes due to the changing tidal levels and/or atmospheric conditions of precipitation and evapotranspiration.

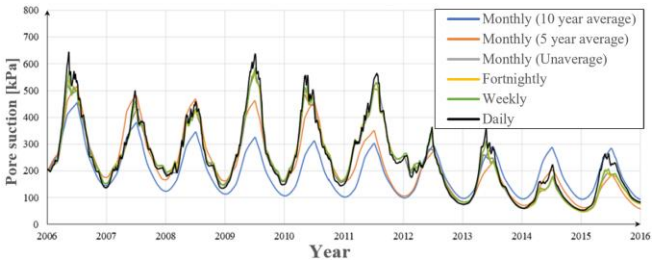

Figure 1. Evolution of pore pressure (suction) on the surface of a London clay column (after Lee, 2019).

Assuming a semidiurnal tidal regime, throughout a typical 50-year lifecycle of a flood embankment, the embankment would experience up to 36,500 tidal cycles. While it may be possible to model all these cycles in a numerical analysis of an embankment lifecycle, such an approach would impose costly computational demands, considering the nonlinearity of material behaviour and of applied boundary conditions. There is therefore a need to devise a simpler, but sufficiently robust and accurate, approach to modelling tidal effects and their impact on flood embankments.

2 BACKGROUND STUDY

A similar concept was explored by Lee (2019), while investigating the impact of applying different time resolutions of the same precipitation and evapotranspiration records, on the stable pore water pressure generated in a column of London clay. Those analyses first applied the actual daily precipitation, over the top surface of the column, from a 10-year rainfall record (2006-2016) at a rain gauge station in Essex, UK (Guo, 2021). The resulting variation of pore water pressure at the column surface is shown in Figure 1, as a benchmark against which to compare subsequent analyses. It should be noted that positive values indicate suctions. The same column was then subjected to similar analyses, but that applied different temporal rainfall discretisation, equivalent weekly, fortnightly, monthly (unaveraged) and monthly averaged rainfall. The resulting surface suctions in Figure 1 (and pore pressures mobilised at depth, not shown here for brevity) indicate that adopting the actual (unaveraged) monthly rainfall was sufficient to capture the general hydraulic behaviour of the analysed column of London clay.

Aggregation of rainfall in a larger monthly time step allows for a more efficient lifecycle analysis that can be performed without losing important characteristic of the general hydraulic behaviour within the soil column. However, it is noted that the case of exploring the impact of an individual storm event would still require the modelling of the storm to be performed in actual (smaller) time steps (Guo, 2021).

In a flood embankment, the presence of semidiurnal tidal cycles and their influence on pore pressure changes around and below the embankment can have significant impact on the embankment. Pore pressure and displacement monitoring of flood embankments along the Thames estuary performed by Marsland (1973) indicated that, in the case of underlying gravels hydraulically connected to the river, tidal lag in the pore pressures within the gravels could occur, weakening the embankment due to uplift. In an embankment that was slowly slipping into the river, Marsland (1973) reported that while the rate of movement was stable, there was a tendency for the rate of movement to increase during periods of higher tides.

Thus there is some evidence that tidal cycles can influence an embankment's behaviour and must be considered in an embankment lifecycle analysis. This requires further investigation to identify the most optimal approach in accurately reproducing tidal cycles and their effects, using time increments larger than hourly. The paper therefore investigates monthly increments, shown as appropriate in the study of Lee (2019).

3 FE SETUP AND ANALYSIS

All finite element (FE) analyses presented here, including the study of Lee (2019), were performed with the FE software ICFEP (Potts and Zdravkovic, 1999).

3.1 FE geometry and analysis

Figure 2 depicts the general geometry of the FE domain used in the analysis, representing an embankment at Dartford built before the great flood of 1953 (Marsland, 1973). The ground level at the embankment site was set at +3.2mOD, with the ground level gradually sloping down to +0.2mOD 50m away from the embankment on the riverward side. The embankment was modelled to 3.1m in height (+6.3mOD), representing an average flood embankment height at Dartford before 1953, with a berm height of 2.5m (+5.7mOD). The embankment base width was 36.4m, while the berm width was 4.2m, with both landward and riverward slopes having a 1V:3H gradient.

The developed FE mesh consisted of 8-noded quadrilateral elements, each node with two displacement degrees of freedom and only the corner nodes with the pore pressure degree of freedom. The analysis was a plane strain hydro-mechanically coupled.

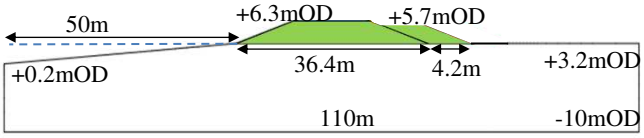

Figure 2. Geometry of the FE domain used in the analysis.

In terms of displacement boundary conditions, both the left and right vertical boundaries restricted horizontal displacements, while the bottom boundary restricted both horizontal and vertical displacements. As for the hydraulic boundary conditions, the left and bottom boundaries were assumed to be impermeable (no flow), while the pore pressure on the right boundary was assumed to remain constant ($\Delta p_f = 0$), assuming far field conditions with the phreatic surface at +2.2mOD. The tidal boundary condition, changing per increment, was applied on the riverward side. One part of the tidal boundary condition is application of pore water pressure on the riverward embankment slope and on the sloping ground surface, according to the tidal elevation of the water level in the river. The second part of the tidal boundary condition is application of total stress along the same boundary, equivalent to the weight of water, in order to achieve a zero effective stress on the tidal boundary. Precipitation and vegetation boundary conditions are applied over the rest of the embankment and ground surface, with further details given in Guo (2021).

The analysis was first initialised with a hydrostatic pore pressure profile in the foundation soil and with a phreatic surface at +2.2mOD, with the embankment elements deactivated. Subsequently, the embankment and berm were constructed in layers, over the span of 1 year, generating excess pore pressures within the foundation soil. After construction of the embankment, precipitation, vegetation and tidal boundary conditions were implemented accordingly in one-month increments.

3.2 Constitutive models

3.2.1 Foundation soil

The soft estuarine foundation soil was modelled using a Modified Cam Clay (MCC) constitutive model (as implemented in ICFEP, Potts and Zdravkovic, 1999), calibrated with undrained triaxial, vane shear, oedometer and moisture content tests, performed on soil specimens collected from a site near the Littlebrook power station in Dartford, along the Thames estuary (Marsland and Powell, 1977). The tests were carried out prior to the construction and testing of a trial embankment at the site.

Figure 3 plots the measured and interpreted undrained shear strength, S_u, profile of the foundation soil vs. depth (Marsland and Powell, 1977), indicting a layer of crust at the surface with an undrained shear strength of around 10kPa on average, before increasing approximately linearly by 4kPa/m from around 3m depth.

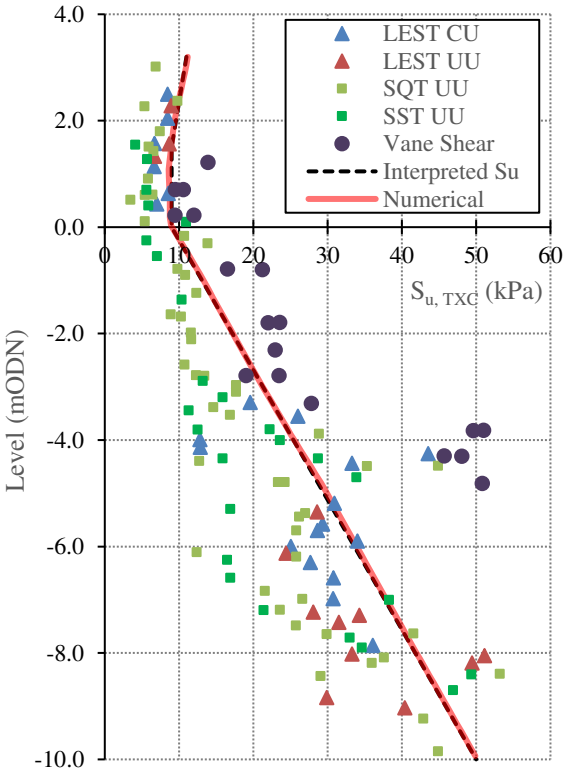

Figure 3. Adopted undrained shear strength profile of the foundation soil, plotted against experimental data from Marsland and Powell (1977).

The coefficient of earth pressure at rest, K_0, was derived by reproducing the initial undrained shear strength profile interpreted in Figure 3, utilising the ability of the MCC model to reproduce the desired S_u profile using Equation (1). This is plotted in Figure 3, together with the undrained triaxial and vane shear tests from Marsland and Powell (1977). The K_0 profile varies linearly from 0.9 at the ground surface to 0.5 at the base of the crust, remaining at 0.5 in depth.

$$S_u = \sigma'_{vi} g(\theta) \cos\theta \cdot \frac{(1+2K_O^{NC})}{6} \cdot (1+B^2) \cdot \left[\frac{2(1+2K_O^{OC})}{(1+2K_O^{NC})OCR(1+B^2)}\right]^{\frac{\kappa}{\lambda}} \quad (1)$$

where θ is the Lode's angle,

$$g(\theta) = \frac{\sin\phi'}{\cos\theta + \frac{1}{\sqrt{3}}\sin\phi' \cdot \sin\theta} \; ; \quad B = \frac{\sqrt{3}(1-K_O^{NC})}{g(\theta)(1+2K_O^{NC})}$$

$$K_O^{OC} = (1-\sin\phi') \cdot OCR^{\sin\phi'}; \; K_O^{NC} = 1-\sin\phi'.$$

The tangent shear modulus, G, of the foundation soil was modelled using the Imperial College Generalised Small Strain Stiffness (ICG3S) model (Taborda et al., 2016), such that the maximum shear modulus increases with the mean effective stress, p', and degrades with increasing deviatoric strain, E_d, according to Equation (2). In the equation, G_0 is the reference shear modulus, G_{min} the minimum shear modulus, m_G the parameter controlling the nonlinearity between G and p', a the degradation parameter for G, R_G is the minimum normalised tangent shear modulus, b is the parameter controlling the nonlinearity of the G degradation, and $n_G = 1$ is the shear modulus scaling factor.

$$G = G_0 \left(\frac{p'}{p'_{ref}}\right)^{m_G} \left(R_G + \frac{(1-R_G)}{1+\left(\frac{|E_d - E_{d,r}|}{n_G \cdot a}\right)^b}\right) \geq G_{min} \quad (2)$$

As the foundation soil at Dartford was not characterised for its small strain stiffness, the shear stiffness was calibrated with data from other similar soils, such as Bothkennar clay. The Bothkennar clay is a soft, silty estuarine clay (Hight et al., 2003) with similar characteristics (in terms of specific gravity, bulk unit weight), and undrained shear strength profile (a thin crust at the top, followed by linearly increasing strength with depth) to the clay in Dartford.

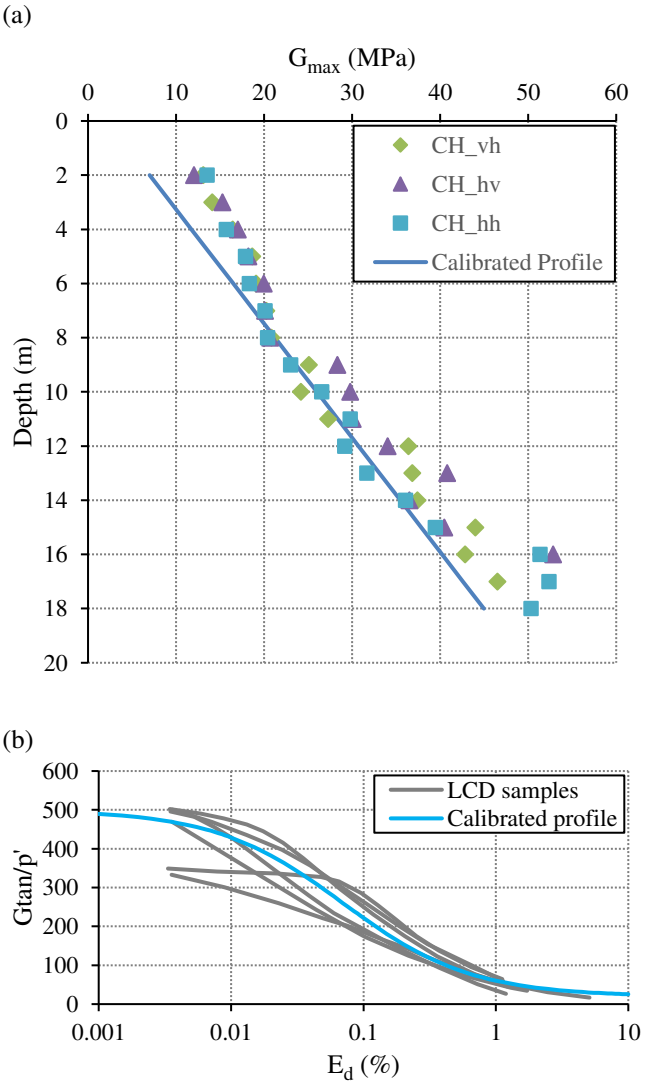

Figure 4. Calibration of shear tangent modulus to Bothkennar clay data from Smith et al. (1992). (a) Maximum shear modulus profile, and (b) Normalised tangent shear modulus degradation curve.

Figure 4(a) plots the calibrated maximum shear modulus profile against the shear moduli of the Bothkennar clay, derived from in-situ geophysics measurements of shear wave velocity (Smith et al., 1992). The field data indicate practically no anisotropy in the measured elastic vertical (G_{vh}, G_{hv}) and horizontal (G_{hh}) shear stiffness components, thus justifying the isotropic interpretation. Figure 4(b) plots the calibrated normalised tangent shear modulus degradation curve, against those obtained from drained probing tests conducted on Bothkennar Clay (Smith et al., 1992). Both graphs indicate good fit to the data. Table 1 summarises the calibrated MCC model parameters adopted in the analysis for the foundation soil.

Table 1. Model parameters of MCC and ICG3S for the foundation soil.

Parameter	Value
Gradient of the normal compression line, λ	0.57
Gradient of the swelling line, κ	0.057
Angle of shearing resistance, $\boldsymbol{\phi'}$	35°
Specific volume of NCL when $p' = 1$ kPa, N	4.39
Maximum shear modulus at p'_{ref}, G_0 (MPa)	50
Reference mean effective stress, p'_{ref} (kPa)	100
Exponent for variation of G_{max} with p', m_G	1
Normalised minimum shear modulus, $R_{G,min}$	0.04
Basic shear modulus degradation parameter, a	0.07
Nonlinearity of shear modulus degradation, b	0.9
Minimum shear modulus, G_{min} (MPa)	2
Permeability, k (m/s)	10^{-8}

3.2.2 Embankment material

The London Clay embankment soil was modelled using the unsaturated Imperial College Single Structure Model (ICSSM, Georgiadis et al. 2005). Confined wetting tests and free swelling tests of London Clay conducted by Monroy et al. (2010) were used in the calibration of the ICSSM. Further details on the calibration of this model for London Clay are detailed in Guo (2021).

The Soil Water Retention (SWR) model of the embankment fill was initially calibrated with drying and wetting curves derived from the London Clay fill specimens by Melgarejo-Corredor (2004). This was subsequently revised based on investigations conducted for a rail infrastructure embankment by Guo (2021), using field estimates of water retention in London Clay embankments. The adopted SWR model was a hysteretic non-linear model, with expressions for the primary drying and wetting curves, respectively, given in Equation (3), Tsiampousi et al. (2013). Table 2 summarises the SWR and permeability parameters adopted for the London Clay fill.

$$S_{r,d} = \frac{1-\frac{s^*}{s_0^*}}{1+a_d \cdot s^*} \quad ; \quad S_{r,w} = \frac{1-\frac{s^*}{s_0^*}}{1+a_w \cdot s^*} \qquad (3)$$

where $S_{r,d}$ and $S_{r,w}$ is the degree of saturation on the primary drying and wetting curve, respectively; $s^* = s - s_{air}$ is the equivalent suction; s_{air} is the air entry value of suction; s_0^* is the equivalent suction at the degree of saturation $S_r = 0$; and a_d and a_w are parameters governing the shape of primary drying and wetting curve, respectively.

Table 2. Parameters of the hysteretic SWR model and isotropic permeability model for the London Clay fill

Parameter	Value
$\boldsymbol{s_{air}}$ (kPa)	5
s_0^* (kPa)	10^9
a_d	$8\text{x}10^{-4}$
a_w	$3\text{x}10^{-3}$
Permeability, k (m/s)	10^{-8}

3.3 Tidal analyses

Based on tidal data, a tidal range of 5.5m (varying from +0.2mOD to +5.7mOD) was assumed for the site, occurring twice daily. To accurately reflect this in the numerical model, the benchmark analysis applied the actual hourly increments, with changing pore pressure and fluid stress boundary conditions on the riverward side for each hour depending on the tidal level, as illustrated in Figure 5. This was repeated over the duration of 30 days, for a total of 720 increments.

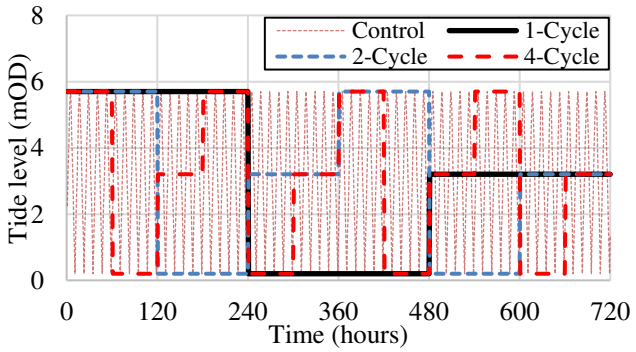

Figure 5. Time series indicating the modelled tide level for each hour of the 4 analyses.

In order to reduce the number of increments and consequently improve on computational efficiency, a high-low-medium cycle of tide level over a given period was proposed, where each stage would be equivalent in time length. For example, in the 1-cycle scenario (black line in Figure 5), high tide would be modelled over 10 days (240 hours), followed by 10 days of low tide, and 10 days of medium tide level. In the 4-cycle scenario, each cycle would last 180 hours, with each stage lasting 60 hours. In terms of numerical increments, each stage was modelled with 2 increments. In this assessment, the 1-cycle, 2-cycle and 4-cycle cases were modelled and their displacements and pore pressures compared with the benchmark analysis.

4 RESULTS AND DISCUSSION

4.1 Displacements

Figures 6(a) and (b) plot the vectors of displacements of the embankment and foundation soil due only to the one month of tidal boundary condition, with Figure 6(a) being the benchmark, and Figure 6(b) the 1-cycle scenario. The vector plots for the 2-cycle and 4-cycle scenarios are similar, but predicting slightly higher maximum displacements of 21.5mm and 22.2mm, respectively, compared to the 1-cycle scenario.

(a) Maximum displacement of 23.4mm

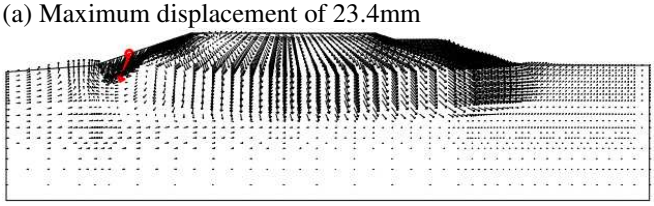

(b) Maximum displacement of 20.7mm

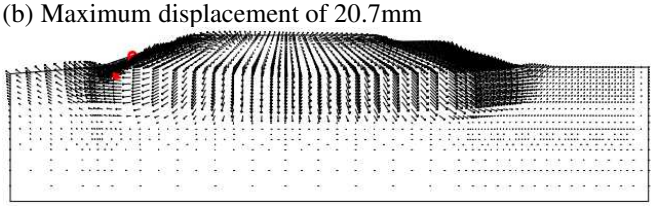

Figure 6. Sub-accumulated displacements after 1 month of tidal boundary condition. (a) Benchmark, (b) 1-cycle.

From Figures 6(a) and (b), it is evident that the 1-cycle (and the 2-cycle and 4-cycle) simplification of the tidal boundary condition is able to reproduce the pattern of displacements similar to benchmark analysis, with only the maximum displacement being underestimated by around 10%. This can be improved by adding more cycles to the month, however, the returns are small, with the 4-cycle scenario reducing the difference to just 5%.

4.2 Pore pressure contours

Figure 7(a) plots the pore pressure contours in the embankment and foundation soil immediately after construction of the embankment and berm. Due to the relatively fast construction in soft clay, excess pore pressures are generated within the foundation, shown by the non-horizontal phreatic surface (i.e. zero pore water pressure contour). In addition, as the tidal and precipitation boundary conditions are not yet active, the embankment pore pressures are entirely in suction.

Figure 7(b) plots the pore pressure contours at the end of the 1 month of tidal boundary conditions in the benchmark analysis, while Figure 7(c) plots those of the 1-cycle scenario. The two figures are nearly identical, except for a very minor difference where the 1-cycle scenario has slightly higher pore pressures beneath the embankment as compared to the benchmark. As for the 2-cycle and 4-cycle scenarios, they also have similar pore pressure contours to the benchmark analysis.

It is worth mentioning that while the final monthly pore pressure contours may be similar between the benchmark and the 1-cycle analyses, the pore pressure contours in the middle of the month are different. Thus, similar to the precipitation aggregation in Lee (2019) study, while taking this simplified 3-stage cycle approach helps the modelling of the general impact of tides on an embankment at the end of the month, the simpler method is unable to capture accurately the pore pressure states in the middle of that month.

(a)

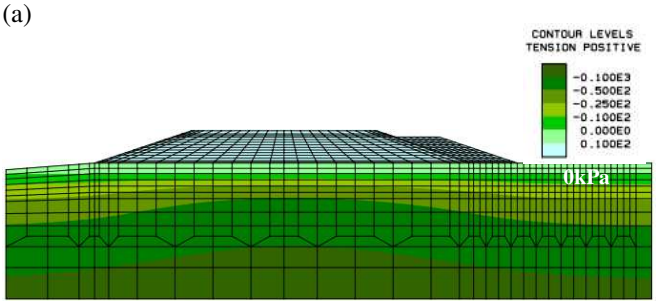

(b)

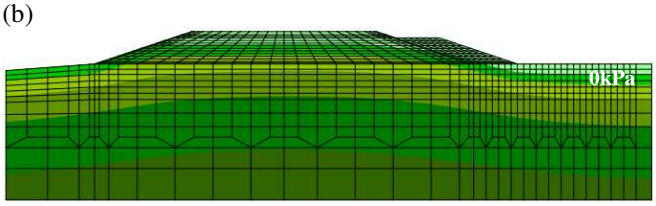

(c)

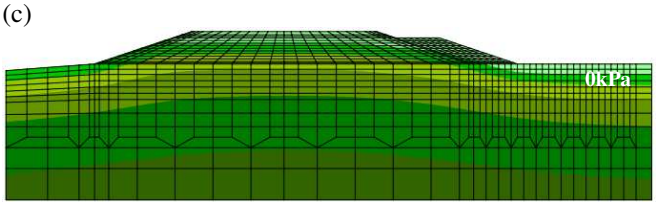

Figure 7. Pore pressure contours within the embankment and foundation soil at (a) End of embankment construction, (b) After 1 month of benchmark tidal boundary condition and (c) After 1 month of simplified 1-cycle tidal boundary condition.

5 CONCLUSIONS

Based on the assessment of displacements and pore pressures in the analyses applying detailed hourly and simplified monthly tidal boundary conditions, it is evident that by adopting even a 1-cycle monthly tidal approach, it is possible to reproduce the impact of hundreds of tidal cycles that the embankment would have experienced. This saves significant amounts of computational effort and time, as the total number of increments can be reduced from 720 (24 times 1-hour increment times 30 days) to just 3.

It should be noted however, that some displacements may be underestimated with the simplified 1-cycle approach. Increasing the number of cycles does increase the maximum displacement, bringing it closer to the benchmark, however, as demonstrated, the returns diminish significantly after a 2-cycle approach.

6 ACKNOWLEDGEMENTS

The work presented in this paper was part of the PhD research of the first author, sponsored by the EPSRC Centre for Doctoral Training in Sustainable Civil Engineering (EP/L016826/1) at Imperial College London and by the Geotechnical Consulting Group LLP. Their support is gratefully acknowledged.

7 REFERENCES

BSI, 2016. BS 6349-1-2: 2016+ A1: 2017. Maritime works. General. Code of practice for assessment of actions.

Georgiadis, K., Potts, D.M., Zdravkovic, L., 2005. Three-Dimensional Constitutive Model for Partially and Fully Saturated Soils. *International Journal of Geomechanics*, *5*(3), 244-255..

Guo, B.W.L., 2021. *Reuse and sustainability of flood defences*; PhD thesis, Imperial College London.

Hight, D.W., Paul, M.A., Barras, B.F., Powell, J.J.M., Nash, D.F.T., Smith, P.R., Jardine, R.J., Edwards, D.H., 2003. The characterisation of the Bothkennar clay. In *Characterisation & Engineering Properties of Natural Soils: Proceedings of the Second International Workshop on Characterisation and Engineering Properties of Natural Soils*, Volume 1, pp.543-597. Singapore. CRC Press.

Lee, J. S., 2019. Assessment of modelling procedure for climate change-induced rainfall events. MEng dissertation, Imperial College London.

Marsland, A., 1973, October. Instrumentation of flood defense banks along the river Thames. In *Proceeding of the British Geotechnical Society Symposium on Field Instrumentation*, held May 30-June 1, 1973 at the Institution Of Electrical Engineers, London.

Marsland A., Powell J. M., 1977. The behaviour of a trial bank constructed to failure on soft alluvium of the River Thames. *Proc. Int. Symp. on Soft Clay*, Bangkok, 505-525.

Melgarejo-Corredor, ML, 2004. Laboratory and numerical investigations of soil retention curves. PhD thesis, Imperial College, University of London.

Monroy, R., Zdravkovic, L., Ridley, A., 2010. Evolution of microstructure in compacted London Clay during wetting and loading. *Géotechnique*, 60(2), pp.105-119.

Potts, D.M., Zdravkovic, L., 1999. *Finite element analysis in geotechnical engineering: Theory*. Thomas Telford Publishing, London, UK.

Smith, P.R., Jardine, R.J., Hight, D.W., 1992. The yielding of Bothkennar clay. Géotechnique, 42(2), pp.257-274.

Taborda, DMG, Potts, DM., Zdravkovic, L. 2016. On the assessment of energy dissipated through hysteresis in finite element analysis. *Computers and Geotechnics* 71:180–94.

Tsiampousi, A., Zdravkovic, L., Potts, D.M. 2013. A three-dimensional hysteretic soil-water retention curve. Geotechnique 63 (2), pp 155-164.